Experimental Thermal and Fluid Science 149 (2023) 110999

Contents lists available at ScienceDirect

Experimental Thermal and Fluid Science

journal homepage: www.elsevier.com/locate/etfs

Experimental study on flashing front propagation in vertical small tubes

Shu-Wen Yue [a,b], Wang-Fang Du [a,b,*], Kai Li [a,b], Xiao Zhao [c], Jian-Fu Zhao [a,b]

[a] CAS Key Laboratory of Microgravity, Institute of Mechanics, Chinese Academy of Science. Beijing 100190, China
[b] School of Engineering Science, University of Chinese Academy of Sciences, Beijing 100049, China
[c] Liaoning Key Laboratory of Complex Energy Conversion and Utilization, School of Energy and Power Engineering, Dalian University of Technology, Dalian 116024, China

ARTICLE INFO

Keywords:
Flashing
Small tube
Flashing front propagation
Sustainability
Velocity

ABSTRACT

Flashing is a classical phenomenon in the discharging process of liquid to the high vacuum environment in space, as well as in nuclear power engineering, chemical engineering, and other engineering fields. To predict the discharge process and ensure the safety of space activities, a better understanding of its laws is needed. In this paper, flashing front propagation in vertical small tubes is experimentally studied under the condition of rapid depressurization. Experiments are carried out with degassed distilled water under different tube diameters and initial temperatures (superheats). The sustainability of flashing front propagation is confirmed to be influenced by superheat, tube diameter and gravity. A correlation is proposed with the Jacob number and Bond number to summarize the sustainability condition. The superficial velocity of flashing front propagation shows to be related to multiple factors such as superheat, tube diameter and downstream pressure. An empirical correlation is proposed to predict the superficial velocity and it agrees well with existing data.

1. Introduction

Generally, “flashing” or “flash evaporation” refers to the intensive liquid–gas phase change phenomenon after liquid undergoes rapid depressurization and then becomes superheated. Flashing has been extensively studied because it is fundamental and decisive in many natural and industry scenarios, such as leakage accidents of pressurized vessels [1,2], seawater desalination [3], fuel atomization [4], spray cooling [5], and even volcanic eruptions [6]. In the liquid discharge process during space flights, flashing strongly influences the flow properties such as pressure and temperature distributions, as well as the discharging time [7]. Furthermore, flashing might even lead to freezing [8,9], which could block the tube and hamper the discharge process.

In a system with a free surface between the liquid and vapor phases, flashing usually occurs in a thin zone near the free surface initially, and then propagates into the superheated liquid as flashing lasts. This thin zone is generally defined as the flashing front, and its propagation process is then called flashing front propagation (FFP) [10]. In some earlier studies, this phenomenon was also called free surface boiling [11], flashing boundary propagation [12], or evaporation wave [13]. Both the secondary nucleation mechanism [14–16] and interfacial instability mechanism [17,18] are thought to account for the self-sustained flashing process on the interface. The secondary nucleation mechanism holds that the rupture of a large bubble entrains gas into the superheated liquid, thus generating many tiny new bubbles. Then these bubbles would grow and rupture again so that the flashing could be sustained. The interfacial instability mechanism holds that Landau instability, Kelvin-Helmholtz instability and Rayleigh-Taylor instability are also responsible for FFP. These two mechanisms may work at the same time. For example, droplets generated by the interfacial instability mechanism would fall back to the liquid surface, causing liquid aeration and stimulating secondary nucleation.

Fritz [19] was one of the earliest researchers who reported the FFP phenomenon. As the pressurized liquid column was suddenly exposed to ambient pressure (101 kPa), an “acceleration front” with a thickness of several centimeters was found to propagate into the bubbly upstream liquid at a nearly constant velocity. Grolmes and Fauske [20] investigated the FFP phenomenon with degassed liquid, while the tube diameter ranges from 2 to 50 mm. The FFP phenomenon without obvious upstream bubbles was observed. The threshold superheat for sustainable propagation was shown as the tube diameter dependent. As the tube diameter increases, the threshold superheat decreases rapidly and then slowly. Das et al. [11] conducted experiments with tube diameter ranges from 30 to 50 mm. They found that both superheat and tube diameter affected the velocity of flashing front. Hill [21] conducted experiments

* Corresponding author at: CAS Key Laboratory of Microgravity, Institute of Mechanics, Chinese Academy of Science. Beijing 100190, China.
E-mail address: duwangfang@imech.ac.cn (W.-F. Du).

https://doi.org/10.1016/j.expthermflusci.2023.110999
Received 25 August 2022; Received in revised form 30 June 2023; Accepted 9 July 2023
Available online 10 July 2023

Nomenclature

Bo	Bond number
Ca	capillary number
C_{pl}	specific heat capacity of liquid at constant pressure (kJ/(kg · K))
D	tube diameter (mm)
g	acceleration of gravity (m/s^2)
H	specific enthalpy (kJ/kg)
Ja	Jacob number
Ja_{th}	threshold Jacob number for sustainable propagation
P	pressure (kPa)
P_{tank}	pressure in vacuum tank (kPa)
t	time (s)
T	temperature (°C)
ΔT	nominal superheat (K)
U_s	superficial velocity (m/s)

Greek symbols

μ	dynamic viscosity (Pa • s)
ξ	liquid–gas density ratio
ρ	density (kg/m^3)
σ	surface tension coefficient (N/m)

Subscripts

0	initial state
1	upstream state
2	downstream state
sat	saturated state
l	liquid phase
v	vapor phase

in a tube with a diameter of 25.4 mm (1 in), the bursts on flashing front was found to be intermittent rather than continuous. Hill suggested that the "boiling front" seen by Das et al. [11] was not associated with liquid fragmentation, and was rather different from that of Grolmes and Fauske [20] and Hill [21].

Simões-Moreira [22] studied FFP in a 15 mm diameter tube with dodecane. Assuming that the downstream was in an equilibrium homogeneous state, Rayleigh equation and Rankine-Hugoniot equation were applied to predict the velocity of the FFP. The prediction agreed well with their experimental results. By allowing velocity slip between the vapor and the liquid film, a more realistic model was proposed by the author [22], and it could theoretically explain the error of the prediction above.

Reinke [2] experimentally investigated FFP with various tube geometrys under a constant outlet pressure of 101 kPa. For tube sizes from 14 to 80 mm, no significant influence of the cross-sectional area on the propagation velocity was noted. A semiempirical correlation was proposed to match the experimental data, in which only superheat and fluid properties are needed. Later, Hahne and Barthau [23] conducted experiments in glass tubes with large diameters ranging from 32 to 252 mm. They indicated that the wall material and discharge area may affect the FFP velocity, but no obvious effect of the tube diameter on sustainable threshold superheat was observed. In the experiments of Graña-Otero and Parra [24], the fluctuation of flashing intensity was observed in cases with low superheat, which is essentially the intermittent flashing phenomenon reported by Hill [21]. Kuznetsov et al. [25] reported a similar phenomenon of flashing intensity pulsations, and they found that the downstream fluid always kept to be nearly saturated during pressure pulsations. More recently, Dewangan and Das [10] conducted FFP experiments under different tube inclinations with a constant tube diameter of 22 mm. The propagation velocity of the flashing front decreased as the tube tends to be horizontal, indicating that gravity also affected the FFP process. In addition, intermittent propagation was also observed in the experiment.

Simulation research on the FFP phenomenon has also been carried out. Harris [26] simulated the flashing front evolution process by a geometrical method. The result produced by secondary nucleation mechanism agreed better with the observation of Hill [21]. Dewangan and Das [27] computationally simulated the propagation of flashing front in the presence of upstream bubble, adopting a one-dimensional, compressible two-phase flow model with diffuse interface. The upstream bubble is noted to slow the propagation of flashing front. Yue et al [28] proposed a modified gas-phase Weber number model for flashing front interfacial area concentration and then introduced it to a two-dimensional mixture model. The simulation superficial velocity of FFP agreed well with their experimental results at a constant tube diameter.

Previous studies indicate that there may be a significant tube diameter effect in the FFP phenomenon while tube diameter is below 15 mm and that FFP may show significant intermittency or gravity dependence under the condition of low or moderate superheat. However, there are few experimental data under condition of small tube diameters and low superheats, which makes it difficult to conduct indepth analysis of the tube diameter effect and the intermittent propagation process. Therefore, further experimental studies under such conditions are needed for a better understanding of FFP phenomenon.

In this paper, FFP experiments are conducted with well-degassed water in an initial temperature range of 20–90 °C and a tube diameter range of 3–14 mm. The main objective of this work is to study the effects of superheat, tube diameter, and tube orientation on the FFP phenomenon, and to reveal the condition of sustainable propagation.

2. Experimental setup

2.1. Experimental platform

An experimental platform (Fig. 1) was built to observe flashing phenomenon. The vacuum system, developed initially by Du et al. [9], was designed to provide a low pressure environment. It is composed of a vacuum tank, a vacuum pump, a vacuum gauge, pipes and valves. The volume of the vacuum tank is approximately 1 m^3, and the pressure inside it will be pumped to less than 0.2 kPa before each test run. Experiments are started by opening the solenoid valve with electrical signal, rather than the traditional way of breaking the diaphragm. The solenoid valve opens fast and steadily, and the opening time is on the order of milliseconds.

The observation system includes the test section, imaging system, and various sensors. The working fluid, i.e., degassed distilled water, is filled in a vertical acrylic tube, which is surrounded by the water bath at a constant temperature. The water column in the vertical tube is approximately 200 mm in length. The vertical tube is connected to the cross tube by a short length of hose. The size of the water bath glass box is 300*300*100 mm. The high-speed camera is installed directly in front of the water bath and is set to be synchronously triggered by the opening signal of the solenoid valve. The focal length of the lens is 12 mm, the frame rate is set to 500 fps, and the pixel size of the image is set to 160*1024 pixels. The spatial resolution of the image is approximately 0.29 mm/pixel. The light source is located behind the water bath and supplies transmitted light for the camera. It consists of a LED array and a light diffusion plate.

To measure the downstream temperature T_2 and pressure P_2, a T-type thermocouple and a pressure transducer are mounted in the cross tube, which is approximately 250 mm above the initial free surface of

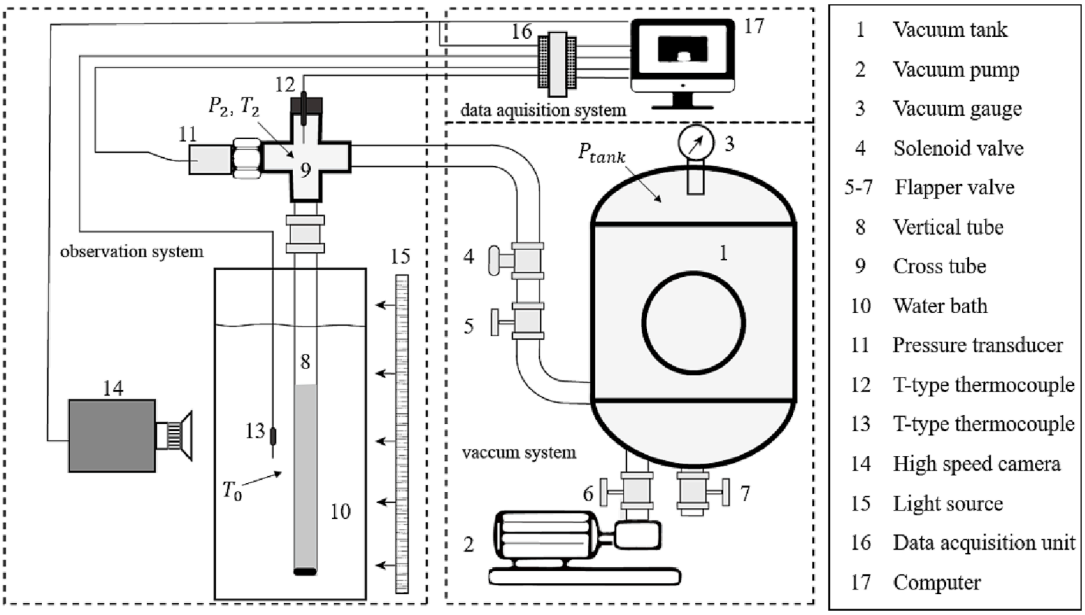

Fig. 1. Schematic diagrams of the experimental platform.

the water column. Another T-type thermocouple is mounted in the water bath and closed to the vertical tube to measure the ambient temperature T_0. The tips of both thermocouples are 20 μm in diameter, and the uncertainty is calibrated as ± 0.5 °C. The pressure transducer has a range of 0–25 kPa with an uncertainty of ± 0.1% full scale at a sampling rate of 1 kHz. The data acquisition unit records the pressure signal at 1 kHz and the temperature signal at 100 Hz.

2.2. Degassing method

Eliminating the influence of upstream noncondensable gas is vital for clear observation of the FFP phenomenon, while it is particularly difficult to ensure the degassing effect [11,13,25,29], especially for experiments with water [10,20]. Generally, upstream noncondensable gas mainly exists in three ways, trapped in wall defects, trapped in tiny bubbles, or dissolved in liquid.

The distilled water was degassed by depressurization after it had been filled into the vertical tube. In this way, the noncondensable gas trapped in wall defects or dissolved in the bulk liquid could be removed at the same time, and the tiny gas bubble entrainment during the liquid filling process could be avoided. However, it is challenging to suppress flashing and to retain the liquid during degassing since the liquid would be blown out of the vertical tube when the superheat becomes high. By trial and error, we found an effective way to degas by gradual depressurization within limited superheat. It was also found that the efficiency could be significantly promoted by continuously tapping the tube during depressurization. Generally, the liquid is fully degassed for several rounds, and each degassing round contains three stages, as shown in Fig. 2.

Preparation stage (from A to B): Adjust the pressure in the vacuum tank (P_{tank}) to slightly above the saturation pressure (P_{sat}) of water corresponding to a temperature of 60 °C. Keep the temperature of the water bath constant at 60 °C.

Rapid depressurization stage (from B to C): Open the solenoid valve, then the pressure of liquid falls suddenly from atmospheric pressure to slightly above P_{sat}.

Slow depressurization stage (from C to D): Keep the vacuum pump working to ensure that the pressure drops slowly and gradually. As the pressure of the liquid falls below P_{sat}, many bubbles appear in the superheated liquid. Tapping the tube continuously can help the bubbles depart from the wall and move up to the surface. To avoid liquid blown out of the test tube, close the solenoid valve to stop the depressurization stage when the pressure is lower than a safe pressure of 15.5 kPa.

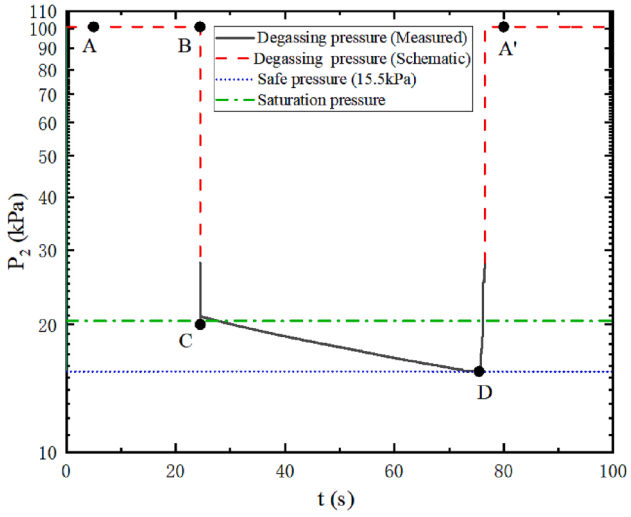

Fig. 2. Demonstration of a typical round of degassing process. T_0 = 60.5 °C,D = 7mm.

Calm stage (from D to A′): Recover the pressure of liquid to atmospheric pressure, preparing for the next turn of degassing or for the experimental run. Bubble formation would stop during this stage.

Before each experimental run, the liquid was degassed carefully for 3–5 rounds until no visible bubble occurred during the slow depressurization stage.

2.3. Experimental procedure

Homogeneous nucleation of pure water is impossible at low temperature without negative pressure [30,31]. Most conditions of the present study fell within this range. For example, Fig. 3 shows the depressurization test, which was carried out just after the degassing process shown in Fig. 2. The highest superheat of water reached in the test is above 55 °C, which is much higher than those in the degassing process. No obvious flashing, however, could be observed in the test.

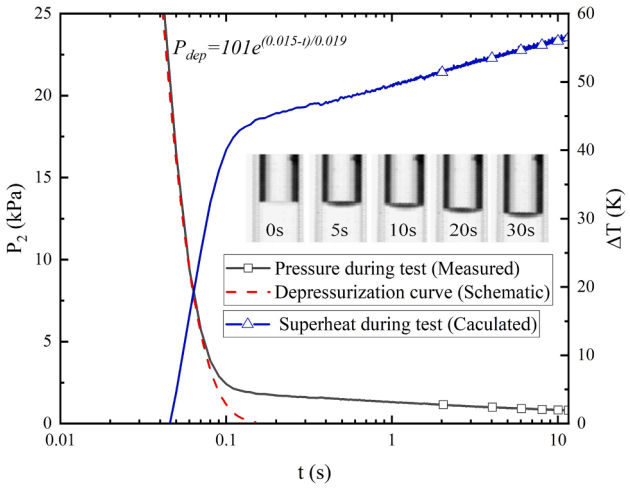

Fig. 3. The pretest on degassing effect. $T_0 = 60.5\,^{\circ}\mathrm{C}, D = 7\mathrm{mm}$.

The liquid remained stable, the surface remained smooth, and the liquid level only dropped very slowly, indicating that evaporation occurred. This result verifies that the degassing method is effective and sufficient to eliminate the effect of upstream noncondensable gas.

Different methods, including knocking the tube wall and presetting a tiny bubble underneath the free surface, were tested to start the flashing process. The latter can provide good repeatability. Therefore, a tiny bubble with a diameter smaller than 1 mm was artificially preset just beneath the initial free surface before each experimental run to provide an initial nucleation site for flashing inception. The experimental process can be summarized as follows:

Fill distilled water into the test tube with an initial level slightly above the required height. The diameter (D) of the test tube used in the present study ranges from 3 mm to 14 mm.

(1) Adjust the temperature of the water bath to 60 °C. Degas water at this temperature.
(2) The water bath was adjusted to the designed initial temperature (T_0) ranging from 20 to 90 °C.
(3) Place a tiny bubble beneath the free surface, and then connect the test tube to the vacuum tank through the cross tube.
(4) Set the high-speed camera ready. The data acquisition unit is started to collect the pressure, temperature, and the triggered signal of both the solenoid valve and the high-speed camera. The triggered signal provides a time synchronization between scientific data and the corresponding images inside the test tube.
(5) Open the solenoid valve to initiate the experimental run. Images inside the test tube are recorded synchronously.

2.4. Image processing process

The gas–liquid interface, as well as the gas–solid interface, may significantly affect the propagation of transmitted light, so the experimental images of the FFP phenomenon are darker in the region of flashing front and downstream. Therefore, the position of the flashing front can be identified by the distribution characteristics of the grayscale of the experimental image.

A program is developed to automatically recognize the position of the flashing front. Since the absolute value of image grayscale is affected by light intensity, here, a relative grayscale is taken to characterize the light transmittance, which is defined as the ratio of grayscale between the tube area and the adjacent background. As shown in Fig. 4, the image processing process is as follows:

Step 1: Select the pixel coordinate range for analysis area A and reference area B according to the position of the vertical tube in the image. The two areas have the same pixel height range.

Step 2: The program calculates the average grayscale at each pixel height for areas A and B. Then calculate the relative grayscale value at each pixel height.

Step 3: The program identifies the position of the flashing front based on the relative grayscale value vs. pixel height curve.

The flashing front position recognized by this method always corresponds to the lowest point of the gas–liquid interface. When a new bubble is generated and grows below the flashing front due to secondary

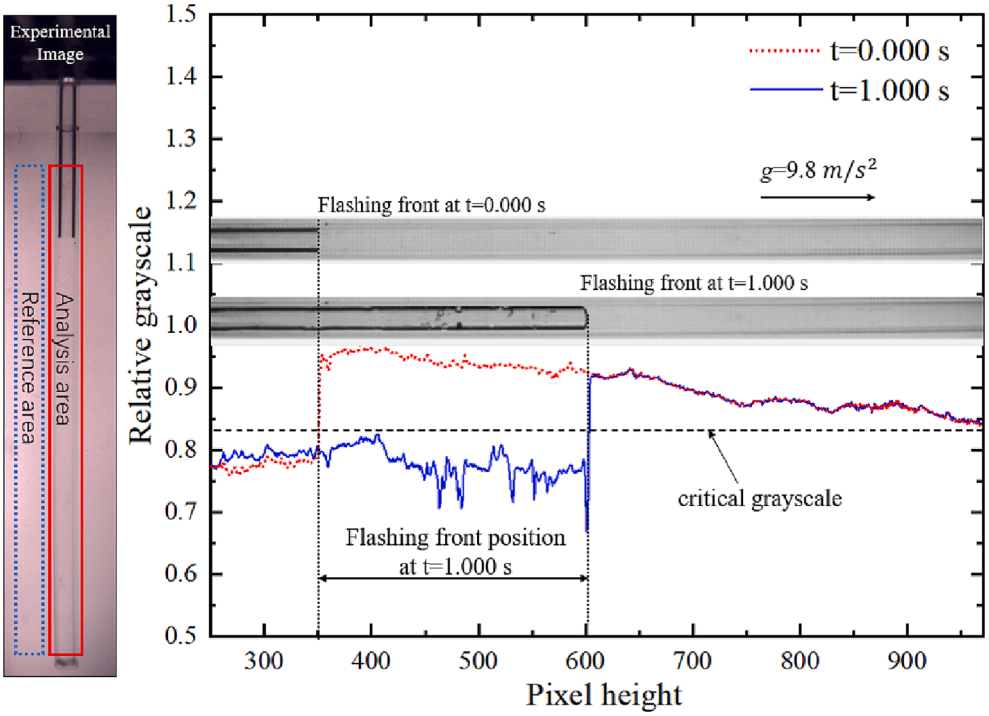

Fig. 4. Flashing front recognition method.

nucleation, the flashing front will be positioned at the lowest point of the bubble edge, and then the recognized position of flashing front will have a jump.

2.5. Data reduction and uncertainty estimation

The superheat at the flashing front is evaluated by the nominal superheat defined as

$$\Delta T = T_0 - T_{sat}(P_2) \tag{1}$$

where $T_{sat}(P_2)$ is the saturated temperature corresponding to downstream pressure P_2.

In general, the characteristic pressure for the FFP process is the local pressure at the flashing front. It is, however, very difficult to measure it without disturbing the flash phenomenon. In some previous research, such as Dewangan & Das [10] and Simões-Moreira [22], P_{tank} was used to characterize the FFP process. It may, however, cause incompatibility between different experimental data due to the significant pressure difference between the test tube and the vacuum tank, which is dependent on the connecting pipeline between them and is usually difficult to measure accurately and/or describe clearly. The measurement point of P_2 is closer to the initial free surface. Thus, we use P_2, instead of P_{tank}, and the nominal superheat defined above to characterize the FFP process in the present study.

The position of the flashing front is defined as the distance between the initial free surface and the lowest point of flashing front. It is converted from the pixel length by image analysis:

$$L = \alpha |L_{pix,0} - L_{pix,f}| \tag{2}$$

where $L_{pix,0}$ and $L_{pix,f}$ are the pixel heights of the initial free surface and the lowest point of the flashing front, respectively, while α is the ratio of physical length to pixel length. Based on the relationship between flashing front position and time, the superficial velocity (U_S) of the FFP can be obtained by linear fitting.

Three dimensionless parameters, namely, the Jacob number, the Bond number, and the capillary number, are used to characterize the FFP process in the present study. The Jacob number based on nominal superheat can be computed from

$$Ja = \frac{C_{pl}\Delta T}{H_{v,2} - H_{l,2}} \tag{3}$$

where the specific heat capacity of liquid at constant pressure C_{pl} is evaluated at the initial liquid temperature. The specific enthalpies $H_{v,2}$ and $H_{l,2}$ are evaluated at the saturated temperature corresponding to P_2.

Analyses on the effect of interface fluctuation and backflow are based on the Bond number, which can be computed from

$$Bo = \frac{\rho_l g D^2}{\sigma} \tag{4}$$

where the liquid density ρ_l and surface tension coefficient σ are evaluated at the initial liquid temperature.

To scale the propagation velocity, the capillary number is introduced as

$$Ca = \frac{\mu_l U_S}{\sigma} \tag{5}$$

where μ_l is the dynamic viscosity of liquid and it is evaluated at the initial liquid temperature.

The measurement accuracy of the primary parameters is summarized in Table 1. According to uncertainty propagation theory, the uncertainty of the indirectly measured parameter Y can be estimated by that of the directly measured parameters $X_1, X_2, X_3, \cdots, X_n$:

Table 1
Uncertainties of primary parameters.

Parameters	Values	Maximum uncertainties
Tube diameter	3–14 mm	±0.1 mm
Pixel height	0–1024 pixel	±1 pixel
Temperature	0–100 °C	±0.5 °C
Pressure in downstream	0.7–20 kPa during FFP	±0.025 kPa
Pressure in tank	0–101 kPa	±25% of measured value

$$\delta Y = \sum_{i=1}^{n} \left| \frac{\partial f}{\partial X_i} \right| \delta X_i \tag{6}$$

The uncertainty of flashing front position is estimated to be within ± 0.6 mm. The uncertainty of nominal superheat is estimated to be within ± 1 K. The uncertainty of Bond number is estimated to be within ± 6.7%. For Jacob number, the uncertainty is within ± 15% during FFP in all cases.

3. Results and discussion

3.1. The inception of the flashing phenomenon

Flashing inception was observed in all experiments with a preplaced tiny bubble, which grew larger and ruptured during depressurization, acting as an active nucleation site and leading to flashing inception. Fig. 5 shows that flashing always occurs near the bubble initially and then spreads across the whole surface and forms the flashing front propagating downward.

Comparing these results with the verifying tests demonstrated in Fig. 3, it is concluded that the threshold superheat for flashing inception strongly depends on the upstream nucleation sites. Therefore, it is very likely that the tube diameter dependence of the self-initiation threshold reported by Grolmes and Fauske [20] might be caused by the diameter dependence of the nucleation site distribution. A similar suggestion was given by Hill [21], who reported a sensitiveness of the threshold superheat on the wall cleanliness.

3.2. The sustainability of FFP

Various states appeared after flashing inception. In some cases, the flashing front could sustain itself and propagate to the end of the test tube, as shown in Fig. 6. However, in other cases, the flashing front would fail to sustain itself, and stop propagating halfway, as shown in Fig. 7.

Fig. 8 summarizes the experimental results on sustainable and unsustainable FFP. Apparently, there is a superheat threshold that determines whether the FFP is self-sustainable or not. The threshold superheat is dependent on the tube diameter. It should be noted that the nominal superheat here is defined as $\Delta T_m = T_0 - T_{sat}(\overline{P}_2)$, in which $\overline{P}_2$ is the mean value of the downstream pressure during propagation.

The interface behaviors and flow characteristics of the FFP under different tube diameters are demonstrated in Fig. 9. Obvious differences existed for different tube diameters. For the largest tube diameter (D = 14 mm), the interface exhibited an intensive fluctuation. Waves with large amplitudes existed along the interface. The downstream region usually appeared very dark compared to the upstream region, indicating strong liquid fragmentation, large amounts of small droplets and intensive flashing. The flashing, however, would sometimes be weakened, showing some weak intermittency. In the case of medium tube diameters (D = 7 mm and 6.5 mm), the interface fluctuation became less significant, but the flashing intermittency was enhanced, and backflow (including downward liquid film flow and even falling liquid fragments) could be observed from time to time. For small tube diameters (D = 5 mm and 3 mm), the interface fluctuation became rather weaker, and a quite smooth surface can be observed. However, the flashing

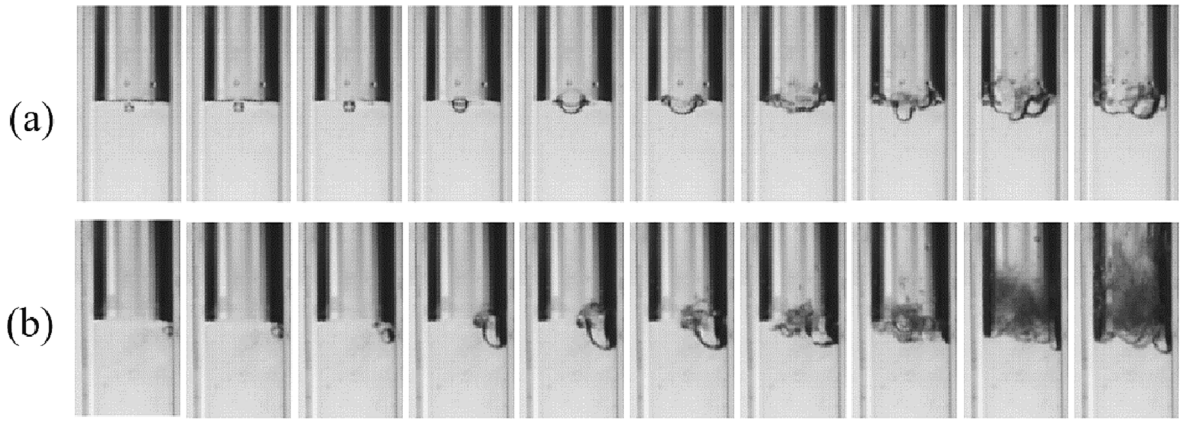

Fig. 5. Flashing inception with preplaced tiny bubble for $D = 14$ mm, shown at a time interval of 4 ms. (a) $T_0 = 39.9°C$. (b) $T_0 = 70.1°C$.

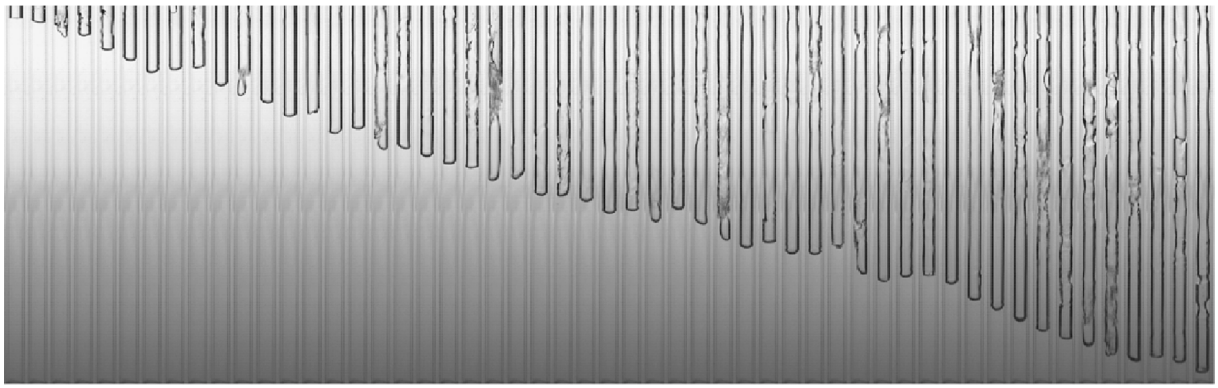

Fig. 6. An example of sustainable FFP. $T_0 = 39.8\,°C$, $D = 7$mm. From 0 to 10.4 s, time interval 0.4 s.

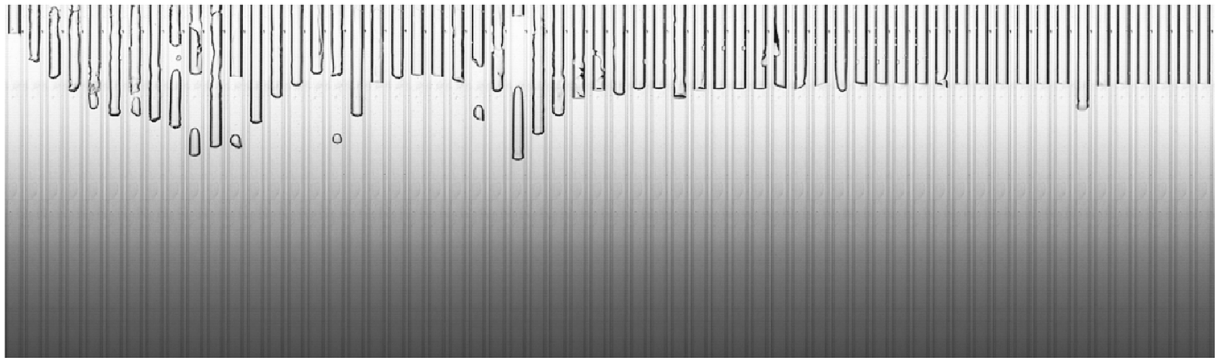

Fig. 7. Example of unsustainable FFP. $T_0 = 20.6°C$, $D = 7$mm. From 0 to 29.5 s, time interval 0.5 s.

intermission became more obvious, even resulting in alternate rise and fall of the liquid column height in the test tube. It was often observed that the downstream tube section was partially or even completely blocked by the falling liquid fragment when flashing paused.

It has also been observed that backflow, especially falling droplets, could lead to secondary nucleation and the restart of flashing, as shown in Fig. 10. The liquid column remained metastable during depressurization at first. A droplet was formed along the tube wall and fell downward. No flashing could be observed before the droplet hit the liquid surface. Approximately 28 ms after the droplet hit the liquid surface, a tiny bubble could be seen just beneath the free surface, which ought to be entrained by the droplet. The tiny bubble then grew and ruptured to start the flashing.

Based on the observations mentioned above, an inference can be obtained that the sustainability of FFP should depend on the secondary nucleation process that induced by the impact of droplets on the surface. The formation of droplets came from the breaking of surface waves and/or the backflow [32–34], and thus was gravity dependent. To verify this inference, experiments with inverted tubes were conducted. As demonstrated in Fig. 11(a), the preexisting bubble exploded and broke the liquid–gas interface after depressurization, thus starting the flashing. The interface, however, returned to become smooth again in the following seconds, and moved upward steadily and slowly. To determine the reason for the interface movement, control experiments with no flashing were also conducted without depressurization, namely at downstream pressure of 101 kPa. Fig. 11(b) shows that the interfaces moved upward at almost the same velocity except for the initial short time. The observations indicate that the flashing front in the inverted

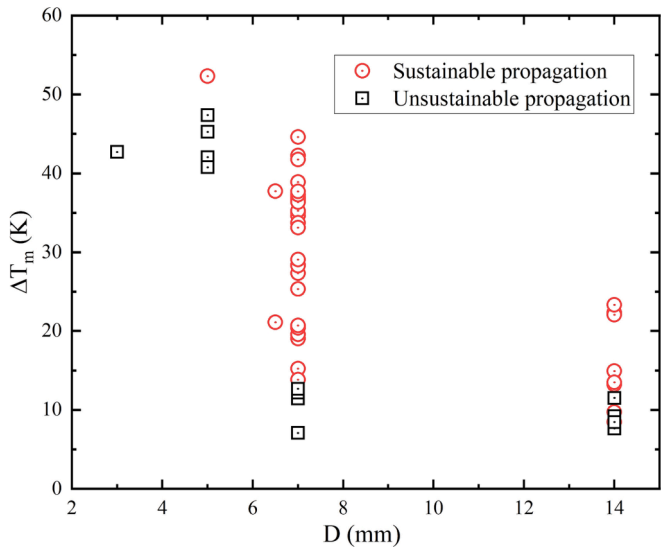

Fig. 8. FFP sustainability under various superheat and tube diameters.

tube failed to sustain itself because no droplet impacted the interface and then no secondary nucleation occurred.

In summary, liquid superheat, tube diameter, and tube orientation relevant to gravity are three key factors that influence the sustainability of FFP. With decreasing tube diameter, the surface tension becomes more dominant, and it suppresses the wave on the interface. This suppresses the inception of flashing both directly owing to the interfacial instability mechanism [17,18] and indirectly owing to the secondary nucleation mechanism [14–16] by reducing the formation of droplets and thus entrained tiny bubbles after their impact on the liquid surface. In addition, a liquid fragment attached to the wall of small tube blocks the entire cross-section easily, rather than falling back and impacting the liquid surface, which further suppresses the inception of flashing. Thus, it is straightforward that the Bond number can be introduced, in addition to the Jacob number, to describe the present observations. Fig. 12 shows an obvious boundary for sustainable FFP, which can be expressed as

$$Ja = 0.1128Bo^{0.82}/(Bo^{0.82} - 2.48)(Bo > 3.5) \quad (7)$$

Here, the Jacob number $Ja = C_{pl}\Delta T_m/(H_{v,2} - H_{l,2})$. The results from Reinke and Yadigaroglu [35] with a tube diameter of 32 mm are also plotted in Fig. 12, and the asymptotic value of 0.1128 in Eq. (7) comes from their observation. It is evident that the sustainable threshold superheat decreases monotonically to a constant as the tube diameter becomes sufficiently large. This trend also agrees well with the experimental results of Grolmes and Fauske [20] and Hahne and Barthau [23].

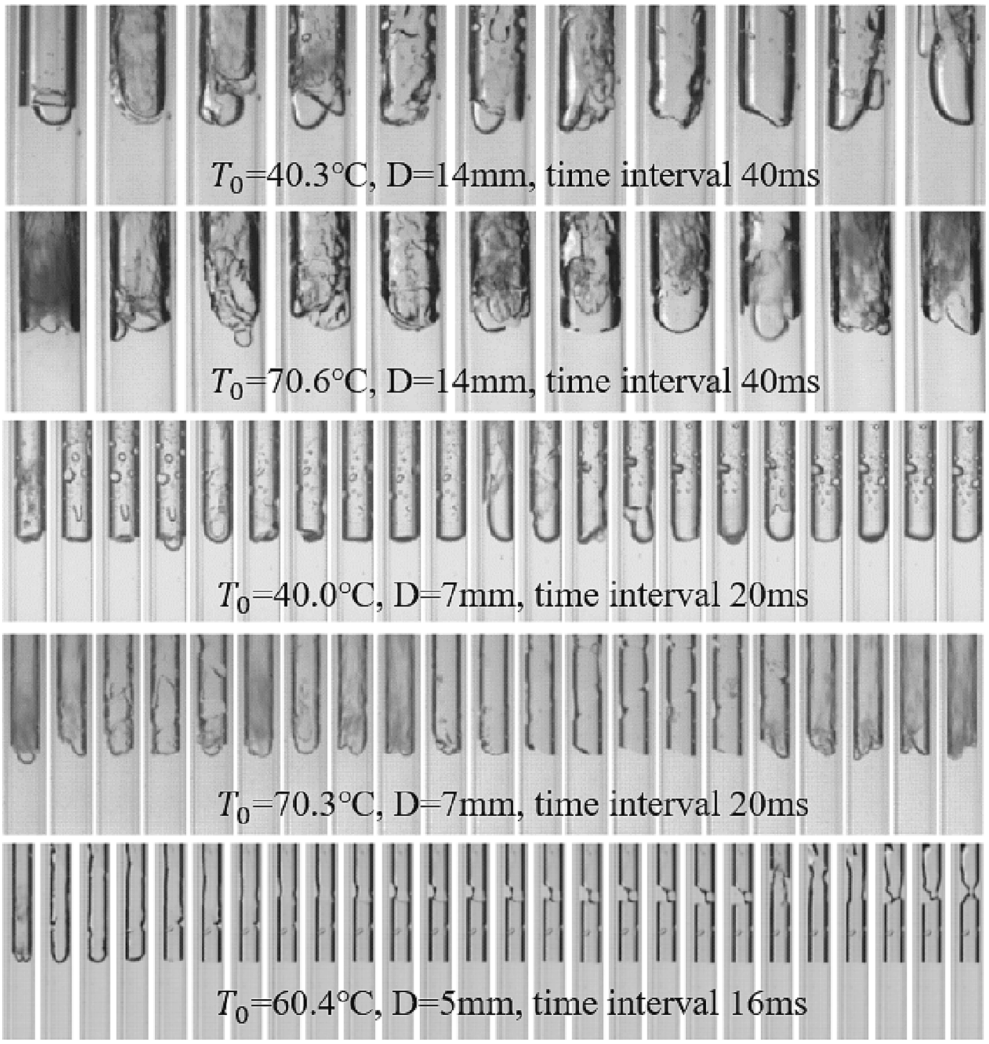

Fig. 9. Interface behaviors and downstream backflow during propagation. The visual field follows the flashing front.

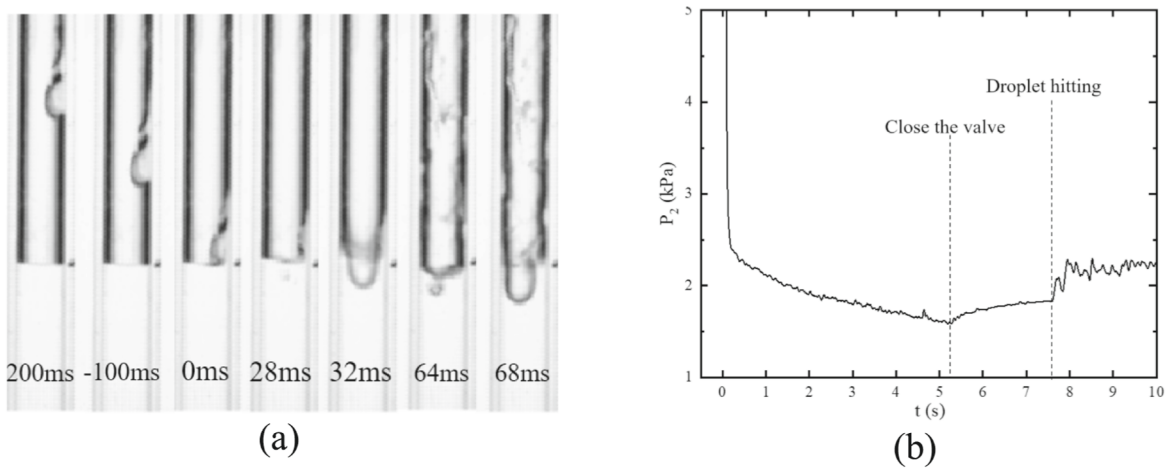

Fig. 10. Flashing started by a falling droplet. $T_0 = 30.1°C$. (a) Phenomenon before and after the falling of liquid. (b) The downstream pressure curve.

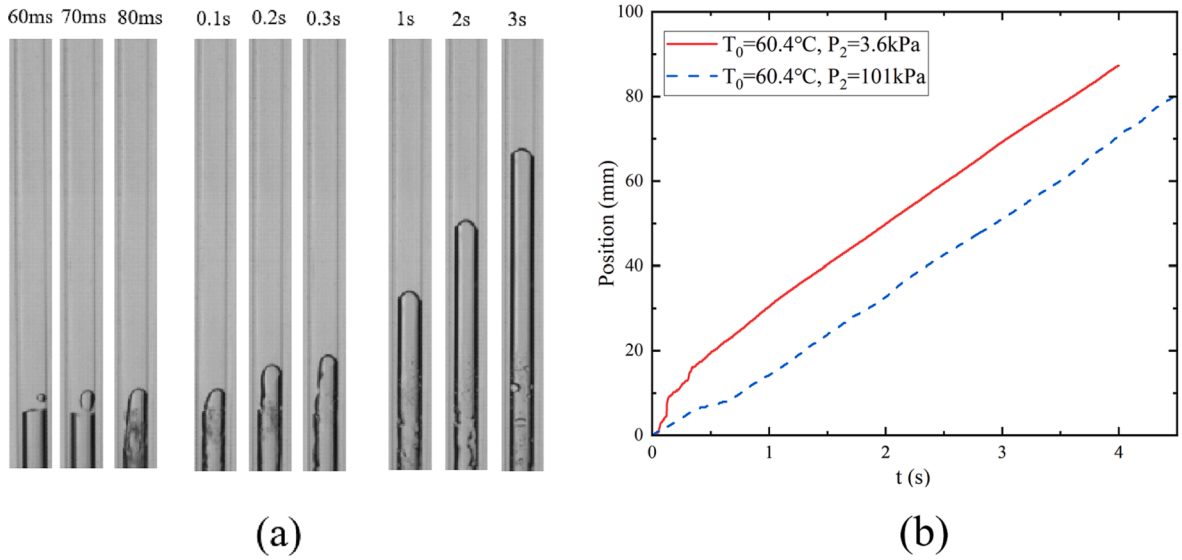

Fig. 11. Unsustainable flashing in an inverted tube.$D = 6.5mm$, $T_0 = 60.4°C$. (a) The phenomenon after depressurization. (b) the position of the interface.

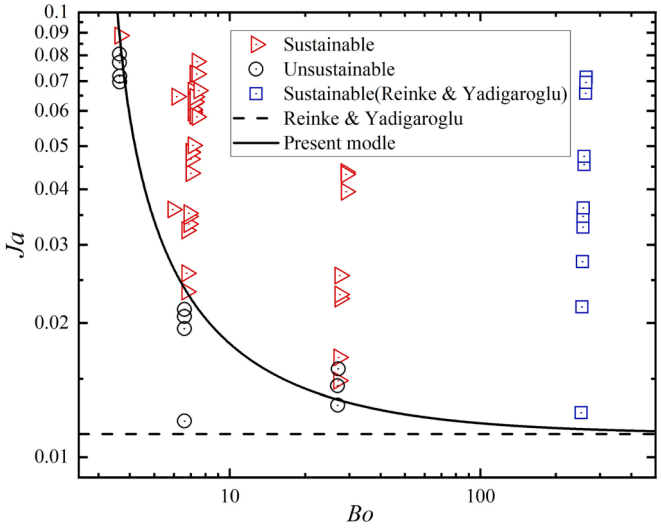

Fig. 12. The sustainable threshold of FFP.

3.3. The velocity of the FFP

The bursts on the flashing front are intermittent rather than continuous during the FFP phenomenon; therefore, the FFP process is locally unsteady [21,24]. As mentioned above, the intermittency of FFP was also observed in the present study. It is obvious in Fig. 13(a) that the downstream region alternates between dark and bright states, indicating that the flashing on the interface alternates between strong and weak states. The corresponding intermittent movement of flashing front is presented in Fig. 13(b). Obviously, the intermittency shows a dependence on the initial temperature, or equivalently the superheat. In the case of a low initial temperature ($T_0 = 30–50$ °C), the propagation was driven by intermittent bubble explosion beneath the free surface in the form of a strong and short burst. Between two successive bursts, significant backflow often occurred, leading to a rise in the liquid level. Overall, the propagation exhibited an alternation of sudden advance, pause, or even slow retreat. In the case of a moderate initial temperature ($T_0 = 60–70$ °C), the flashing front could propagate continuously for hundreds of milliseconds, indicating that continuous flashing occurred and that the flashing might be caused by secondary nucleation under the action of bubble burst. The intermittency also became weaker, and only weak backflow occurred. The liquid fragment attached to the tube wall

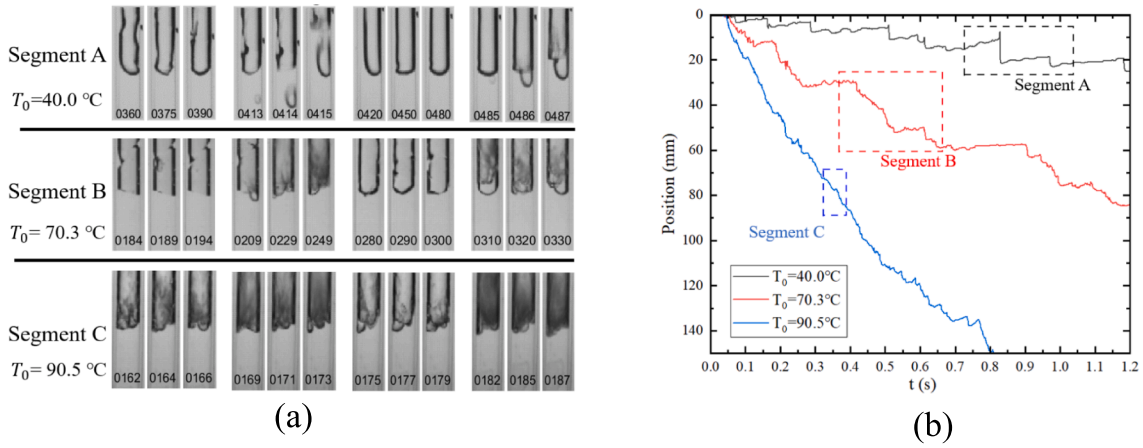

Fig. 13. The FFP intermittency for $D = 7$ mm. (a) The alternation of strong and weak flashing. The visual field follows the flashing front. The frame number is marked in each picture. (b) The position of the flashing front.

exploded and flowed upward before falling into the free surface. In the case of high initial temperature (T_0 = 80–90 °C), there was no obvious pause and the propagation exhibited nearly a continuous advance mode with an alternation of acceleration and deceleration.

Fig. 14 shows typical flashing front position vs. time curves under different tube diameters. As the tube diameter decreases, the fluctuation of curves weakens, the time between two successive bursts increases, and the intermittency becomes more significant. Especially when the tube diameter decreases to 5 mm, the time during two successive bursts reaches the order of 1 s, leading to a significant slowdown in propagation.

It is noted that there existed notable differences compared to previous studies reported in the literature. Hill [21] observed a waiting time on the order of 1 ms between two successive bursts with a large Bond number above 800 and a Jacob number (defined with pressure in reservoir) above 0.2. In the present study, the waiting time between two successive bursts could be up to hundreds of milliseconds, showing a much stronger intermittency. And during the long waiting period, the influence of backflow is more significant. As observed and analyzed earlier, the great difference in the effect of tube diameter should account for the differences of phenomena. The narrow space of the cross-section of small tubes used in the present study suppresses the wave on the interface and then the formation of droplets. This would result in a lower frequency of the occurrence of secondary nucleation at an equivalent or lower superheat.

Although locally irregular, the propagation of the flashing front can be well characterized with a superficial velocity (U_s). Fig. 15 shows the superficial velocities for different initial liquid temperatures (T_0) and

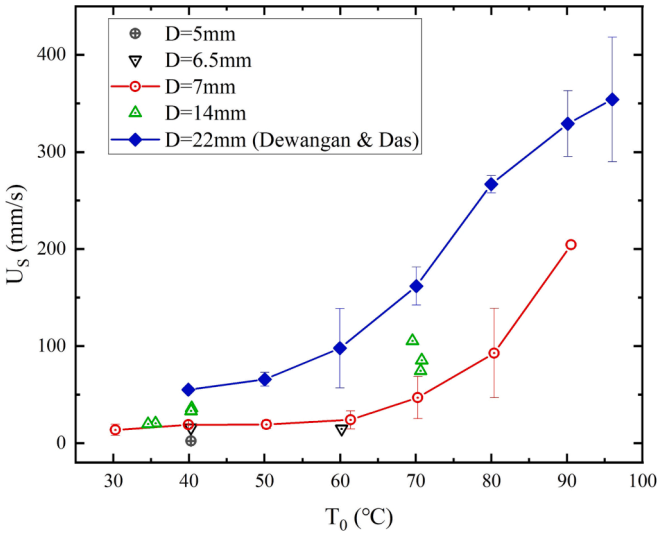

Fig. 15. Superficial velocity under different initial temperatures and tube diameters.

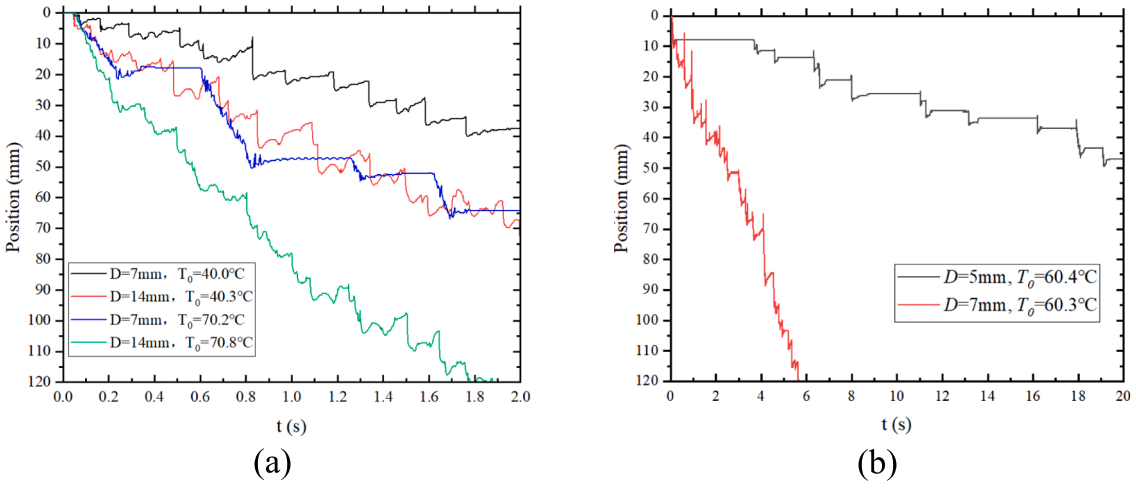

Fig. 14. Typical flashing front position vs. time curve under various tube diameters.

tube diameters (D). It also indicates the data of $D = 22$ mm from Dewangan and Das [10]. In general, the superficial velocity increased with increasing initial liquid temperature and tube diameter.

The following semiempirical correlation was proposed by Reinke and Yadigaroglu [35] to predict the superficial velocity of the FFP

$$Ca = 0.0813(Ja - Ja_{th}) \tag{8}$$

where the threshold Jacob number Ja_{th} corresponds to the sustainable threshold superheat suggested as approximately 5.8 °C [35]. As shown in Fig. 16, this correlation fits well with their own data with a diameter of 40 mm and an outlet pressure of 101 kPa. However, it overestimates the FFP velocity for the present study and those of Dewangan and Das [10]. It is noted that the data from Dewangan and Das [10] are actually shown with a different definition of the superheat, which is based on the pressure of the vacuum tank rather than the downstream pressure because no data of the downstream pressure were provided except for one case. The modified data point for this case was also shown in Fig. 16 based on the same definition in the present study. Overestimation of the correlation of Reinke and Yadigaroglu [35] has not changed in essence.

To better fit the experimental data, the influences of the downstream gas–liquid density ratio $\xi = \rho_{v,2}/\rho_{l,2}$ and the dependence of the threshold Jacob number Ja_{th} on the Bond number were taken into consideration, and then a new correlation could be proposed as

$$Ca = 0.85(Ja - Ja_{th})^{0.24}\xi^{0.69} \tag{9}$$

where the threshold Jacob number Ja_{th} was calculated by Eq. (7).

All sets of data were divided into two groups to evaluate the prediction accuracy. In the first group, data satisfies the condition of $Ja - Ja_{th} > \lambda$ and they are more reliable, where λ is the Jacob number corresponding to ΔT_m of 1 K. In the other group named the near-critical cases herein, data points are too close to the boundary of the sustainable FFP, which may cause greater deviation. A better performance of the new correlation, namely Eq. (9), is shown in Fig. 17. In general, more than 70% of the sets of data, which covered a wide range of tube diameters, initial temperatures, and downstream pressures, were located inside the ± 50% error line.

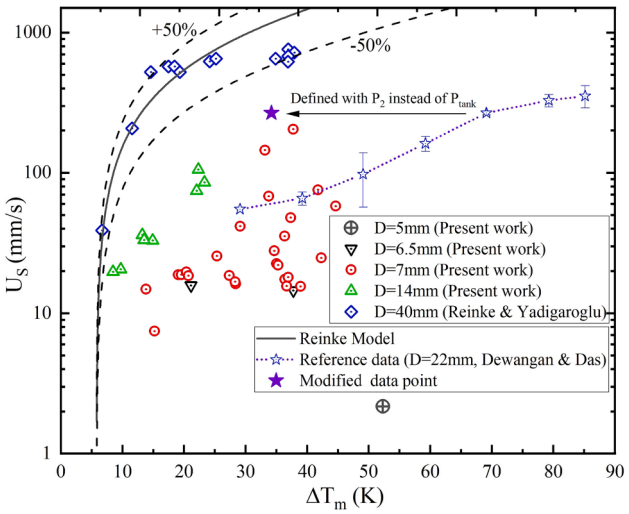

Fig. 16. Superficial velocity under different nominal superheats.

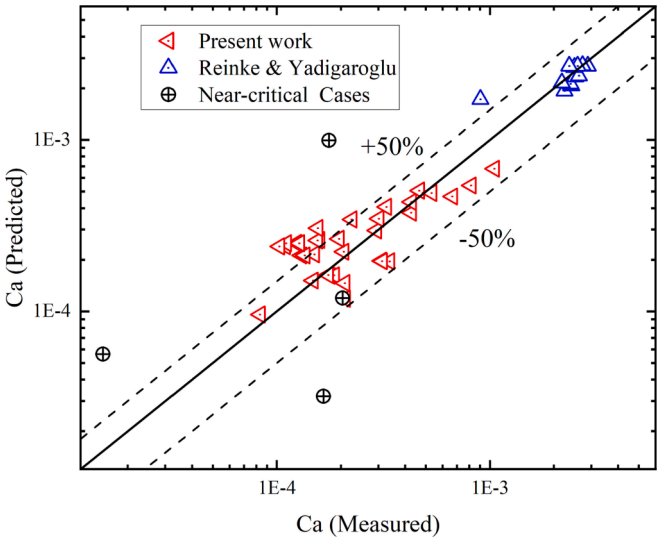

Fig. 17. Prediction with the present model.

4. Conclusion

Experiments were performed to improve the understanding of flashing front propagation of water in small tubes. An artificial bubble was preplaced beneath the free surface as a nucleation site. Flashing occurred near the bubble after depressurization and then spread to the entire free surface, thus forming the flashing front. The following are the key conclusions of the study.

(1) Flashing front propagation could be self-sustainable or unsustainable. Superheat, tube diameter and gravity are the key factors that affect sustainability. For upward tubes, there is a diameter-correlated threshold superheat below which the FFP would be unsustainable.
(2) The superficial velocity of the FFP increases with increasing initial temperature and tube diameter.
(3) The parameter ξ representing the downstream gas–liquid density ratio was introduced to account for the influence of the downstream pressure. A new empirical correlation of the dimensionless superficial velocity of the FFP was obtained based on ξ, Ja and Ja_{th}. It agrees well with the experimental data in a wide range.

CRediT authorship contribution statement

Shu-Wen Yue: Conceptualization, Methodology, Software, Investigation, Data curation, Formal analysis, Writing – original draft. **Wang-Fang Du:** Conceptualization, Funding acquisition, Resources, Supervision, Writing – review & editing. **Kai Li:** Supervision, Resources. **Xiao Zhao:** Methodology, Writing – review & editing. **Jian-Fu Zhao:** Conceptualization, Project administration, Supervision, Writing – review & editing.

Declaration of Competing Interest

The authors declare that they have no known competing financial interests or personal relationships that could have appeared to influence the work reported in this paper.

Data availability

Data will be made available on request.

Acknowledgements

This work was financially supported by the Key Research Program of Frontier Sciences / CAS under the grant of QYZDY-SSW-JSC040, and the National Natural Science Foundation of China (NSFC) under the grant of 11802314.

References

[1] J. Casal, Evaluation of the effects and consequences of major accidents in industrial plants, Elsevier, Amsterdam (2008), https://doi.org/10.1016/S0921-9110(08)80002-X.

[2] P. Reinke, Surface boiling of superheated liquid, Paul Scherrer Institute, 1997. Ph. D. thesis.

[3] M. Maria Antony Raj, K. Kalidasa Murugavel, T. Rajaseenivasan, K. Srithar, A review on flash evaporation desalination, Desalin, Water Treat. 57 (29) (2016) 13462–13471.

[4] J. Senda, Y. Wada, D. Kawano, H. Fujimoto, Improvement of combustion and emissions in diesel engines by means of enhanced mixture formation based on flash boiling of mixed fuel, Int. J. Engine Res. 9 (1) (2008) 15–27, https://doi.org/10.1243/14680874JER02007.

[5] W.L. Cheng, W.W. Zhang, H. Chen, L. Hu, Spray cooling and flash evaporation cooling: The current development and application, Renew. Sustain. Energy Rev. 55 (2016) 614–628, https://doi.org/10.1016/j.rser.2015.11.014.

[6] Y.X. Zhang, B. Sturtevant, E.M. Stolper, Dynamics of gas-driven eruptions: Experimental simulations using CO2-H2O-polymer system, J. Geophys. Res. 102 (B2) (1997) 3077–3096, https://doi.org/10.1029/96JB03181.

[7] D.W. Wang, K. Xu, X.W. Ning, J.F. Zhao, J.Y. Miao, C.Y. Niu, Ground simulation test for the working fluid evacuation in high vacuum and low gravity environment, Spacecr. Environ. Eng. 36 (3) (2019) 257–263.

[8] K.X. Zhao, J.F. Zhao, S.L. Chen, W.F. Du, Thermodynamics of flashing/freezing process of a droplet in vacuum, Chinese J. Sp. Sci. 31 (1) (2011) 57–62.

[9] W.F. Du, J.F. Zhao, K. Li, Experimental study on thermal-dynamical behaviors of liquid droplets during quick depressurization, J. Eng. Thermophys. 33 (8) (2012) 1349–1352.

[10] K.K. Dewangan, P.K. Das, Experimental analysis of flashing front propagation in superheated water - Effects of degree of superheat, tube inclination, and secondary nucleation, Phys. Fluids 32 (7) (2020), 073311, https://doi.org/10.1063/5.0006840.

[11] P.K. Das, G.S. Bhat, V.H. Arakeri, Investigations on the propagation of free surface boiling in a vertical superheated liquid column, Int. J. Heat Mass Transf. 30 (4) (1987) 631–638, https://doi.org/10.1016/0017-9310(87)90193-1.

[12] Y.V. Fairuzov, Blowdown of Pipelines Carrying Flashing Liquids, AIChE J. 44 (2) (1998) 245–254, https://doi.org/10.1002/aic.690440203.

[13] P.M. Hansen, A.V. Gaathaug, D. Bjerketvedt, K. Vaagsaether, The behavior of pressurized liquefied CO2 in a vertical tube after venting through the top, Int. J. Heat Mass Transf. 108 (2017) 2011–2020, https://doi.org/10.1016/j.ijheatmasstransfer.2017.01.035.

[14] R. Mesler, G. Mailen, Nucleate boiling in thin liquid films, AIChE J. 23 (6) (1977) 954–957, https://doi.org/10.1002/aic.690230629.

[15] K. Carroll, R. Mesler, Part II: Bubble entrainment by drop-formed vortex rings, AIChE J. 27 (5) (1981) 853–856, https://doi.org/10.1002/aic.690270525.

[16] J. Sigler, R. Mesler, The behavior of the gas film formed upon drop impact with a liquid surface, J. Colloid Interface Sci. 134 (2) (1990) 459–474, https://doi.org/10.1016/0021-9797(90)90156-I.

[17] A. Prosperetti, M.S. Plesset, The stability of an evaporating liquid surface, Phys. Fluids 27 (7) (1984) 1590–1602, https://doi.org/10.1063/1.864814.

[18] F.J. Higuera, The hydrodynamic stability of an evaporating liquid, Phys. Fluids 30 (3) (1987) 679–686, https://doi.org/10.1063/1.866372.

[19] G. Friz, Coolant ejection studies with analogy experiments, in: Proceeding Conference on Safety Fuels and Core Design in Large Fast Power Reactors, 1965: pp. 890–894.

[20] M.A. Grolmes, H.K. Fauske, Axial propagation of free surface boiling into superheated liquids in vertical tubes, in: 5th International Heat Transfer Conference, 1974. https://doi.org/10.1615/IHTC5.140.

[21] L.G. Hill, An experimental study of evaporation waves in a superheated liquid, California Institute of Technology, 1991. Ph.D. thesis. https://doi.org/10.1007/978-3-642-83587-2_3.

[22] J.R. Simões-Moreira, Adiabatic Evaporation Waves, Rensselaer Polytechnic Institute, 1994. Ph.D. thesis.

[23] E. Hahne, G. Barthau, Evaporation waves in flashing processes, Int. J. Multiph. Flow. 26 (4) (2000) 531–547, https://doi.org/10.1016/S0301-9322(99)00031-2.

[24] J.C. Graña-Otero, I.E. Parra, Experimental results on evaporation waves, Defect Diffus, Forum. 312–315 (2011) 635–640, https://doi.org/10.4028/www.scientific.net/DDF.312-315.635.

[25] V.V. Kuznetsov, I.A. Kozulin, O.V. Vitovsky, Experimental investigation of adiabatic evaporation waves in superheated refrigerants, J. Eng. Thermophys. 21 (2) (2012) 136–143, https://doi.org/10.1134/S1810232812020051.

[26] L.D. Harris, An analysis of the propagation mechanism for rapid evaporation waves, University of Toronto, 2006. Ph.D. thesis.

[27] K.K. Dewangan, P.K. Das, Numerical simulation of flash evaporation in the presence of secondary nucleation, Int. J. Multiph. Flow 142 (2021) 103703.

[28] S.W. Yue, W.F. Du, K. Li, J.F. Zhao, Numerical study on flashing front propagation phenomenon in vertical tube, Chinese J. Theo. Appl. Mech. 55 (8) (2023) 1–10, https://doi.org/10.6052/0459-1879-23-115.

[29] P. Reinke, Site deactivation techniques for suppression of nucleation in superheated liquid, Exp. Heat Transf. 10 (2) (1997) 133–140, https://doi.org/10.1080/08916159708946539.

[30] Q. Zheng, D.J. Durben, G.H. Wolf, C.A. Angell, Liquids at large negative pressures: Water at the homogeneous nucleation limit, Science 254 (5033) (1991) 829–832, https://doi.org/10.1126/science.254.5033.829.

[31] F. Caupin, E. Herbert, Cavitation in water: a review, Comptes Rendus Phys. 7 (9–10) (2006) 1000–1017, https://doi.org/10.1016/j.crhy.2006.10.015.

[32] D.C. Blanchard, A.H. Woodcock, Bubble formation and modification in the sea and its meteorological significance, Tellus 9 (2) (1957) 145–158, https://doi.org/10.1111/j.2153-3490.1957.tb01867.x.

[33] H.C. Pumphrey, P.A. Elmore, The entrainment of bubbles by drop impacts, J. Fluid Mech. 220 (1990) 539–567, https://doi.org/10.1017/S0022112090003378.

[34] J.C. Bird, R. De Ruiter, L. Courbin, H.A. Stone, Daughter bubble cascades produced by folding of ruptured thin films, Nature 465 (7299) (2010) 759–762, https://doi.org/10.1038/nature09069.

[35] P. Reinke, G. Yadigaroglu, Explosive vaporization of superheated liquids by boiling fronts, Int. J. Multiph. Flow 27 (9) (2001) 1487–1516, https://doi.org/10.1016/S0301-9322(01)00023-4.l.